THE JOURNAL OF PHYSICAL CHEMISTRY C

ARTICLE

pubs.acs.org/JPCC

Effect of Vanadium Incorporation on Electrochemical Performance of $LiFePO_4$ for Lithium-Ion Batteries

Lu-Lu Zhang,[†] Gan Liang,[‡] Alexander Ignatov,[§,⊥] Mark C. Croft,[§,⊥] Xiao-Qin Xiong,[†] I-Ming Hung,[¶] Yun-Hui Huang,[*,†] Xian-Luo Hu,[†] Wu-Xing Zhang,[†] and Yun-Long Peng[†]

[†]State Key Laboratory of Materials Processing and Die & Mold Technology, School of Materials Science and Engineering, Huazhong University of Science and Technology, Wuhan, Hubei 430074, China

[‡]Department of Physics, Sam Houston State University, Huntsville, Texas 77341, United States

[§]Department of Physics and Astronomy, Rutgers University, Piscataway, New Jersey 08854, United States

[⊥]NSLS, Brookhaven National Laboratory, Upton, New York 11973, United States

[¶]Yuan Ze Fuel Cell Center/Department of Chemical Engineering and Materials Science, Yuan Ze University, No. 135, Yuan-Tung Road, Chungli, Taoyuan 320, Taiwan

ABSTRACT: A series of $LiFe_{1-x}V_xPO_4/C$ samples have been successfully prepared using a two-step solid-state reaction route. The effect of vanadium incorporation on the performance of $LiFePO_4$ has systematically been investigated with X-ray diffraction, Raman spectroscopy, charge/discharge measurements, and cyclic voltammetry tests. It is found that V incorporation significantly enhances the electrochemical performance of $LiFePO_4$. Particularly, the $LiFePO_4/C$ sample with 5 at. % vanadium doping exhibits the best performance with a specific discharge capacity of 129 mAh g^{-1} at 5.0 C after 50 cycles; the capacity retention ratio is higher than 97.5% at all C rates from 0.1 to 5.0 C. X-ray absorption spectroscopy results show that the valence of V in $LiFe_{0.95}V_{0.05}PO_4/C$ is between +3 and +4. It is confirmed that the samples with $x \leq 0.03$ are in single phase, whereas the samples with $0.05 \leq x < 1.00$ contain two impurity phases: $Li_3V_2(PO_4)_3$ and $LiVOPO_4$. A clear feature of vanadium incorporation in $LiFePO_4$ has been specified.

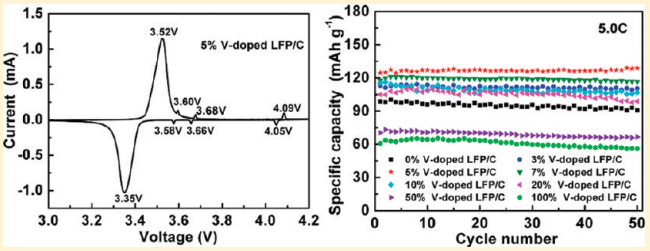

INTRODUCTION

Because of rapid depletion of fossil fuels and serious environmental pollution caused by automobiles, more attention has been focused on electric vehicles (EVs) or hybrid electric vehicles (HEVs). Lithium-ion batteries (LIBs) are the key power source for EVs or HEVs. For LIBs, the reversible capacity strongly depends on the cathode material. Olivine-type $LiFePO_4$ is regarded as one of the most promising cathode materials due to its high theoretical capacity (170 mAh g^{-1}), low cost, nontoxicity, and environmental friendliness.[1] However, $LiFePO_4$ usually shows a poor rate capability because of its low intrinsic electronic conductivity ($\sim 10^{-9}$ S cm^{-1}) and slow lithium-ion diffusion.[2−4] Accordingly, great efforts have been devoted to improving the rate performance of $LiFePO_4$, and successful results showed that carbon coating[5−9] or utilization of nanosized electrode materials[10−13] is very efficient, but the tap density drops dramatically when the carbon content increases and/or particle size decreases. Therefore, doping with supervalent cations[7,14−18] is commonly used for the modification of $LiFePO_4$ without tap density reduction. Regarding this, vanadium modification is a hotspot because V can form a number of electrochemically active compounds, such as V_2O_5,[19] $Na_3V_2(PO_4)_2F_3$,[20,21] $VOPO_4$,[22] $LiVPO_4F$,[23] β-$LiVOPO_4$,[24] and $Li_3V_2(PO_4)_3$,[25−29] which can intercalate/deintercalate lithium reversibly. Wen et al.[30] obtained a reversible capacity of 130 mAh g^{-1} at a charge−discharge current of 80 mA g^{-1} in $LiFe_{0.9}V_{0.1}PO_4$ prepared via a solid-state reaction. Liu et al.[31] found that doping with a heteroatom (Ti, Zr, V, Nb, and W) could promote the performance of $LiFePO_4$ at high current due to the enlarged lattice volume that provides more space for lithium-ion transfer. Yang et al.[32] and Sun et al.[33] confirmed with Rietveld refinement that V replaced Fe in the $LiFePO_4$ matrix structure. However, Hong et al.[34] found that vanadium in $LiFeP_{0.95}V_{0.05}O_4$ was incorporated into the olivine structure at the phosphorus site instead of the iron site. Wu et al.[35] synthesized a multidoped $LiFePO_4/C$ with Mn, V, and Cr ions by using steel slag as a raw material. As compared with undoped $LiFePO_4/C$ prepared only from chemical reagents, the multidoped $LiFePO_4/C$ exhibited a better rate capability due to the improvement of the electrode reactivity by multidoping particularly at high rates. Jin et al.[36] also found that introduction of a small amount of vanadium into the carbon-coated $LiFePO_4$ particles led to significant improvement in rate capability and low-temperature performance, which was attributed to the formation of conductive V_2O_3 nanograins. Recently, Ma et al.[37] studied the effect of vanadium on physicochemical and electrochemical

Received: April 14, 2011
Revised: June 5, 2011
Published: June 08, 2011

performances of $LiFePO_4$ and observed that, at different V-doping levels, different impurity phases (VO_2 or $Li_3V_2(PO_4)_3$ phases) can be formed. It is noted that $Li_3V_2(PO_4)_3$ is also a promising cathode material with a high operating voltage (up to 4.0 V). Moreover, it exhibits faster Li^+-ion migration than $LiFePO_4$ due to its open three-dimensional (3D) framework. Despite the above-mentioned progress, it is still controversial about whether vanadium can be doped into the crystal structure of $LiFePO_4$. Nevertheless, with a low doping level of vanadium, the electronic conductivity and electrochemical performance of $LiFePO_4$ were always enhanced.[28,32,37,38] Because V doping into the crystal structure of $LiFePO_4$ or the formation of vanadium compound impurities is a promising way to improve the electrochemical performance, it is highly desirable to investigate the valence of V in these compounds.

In the present work, we prepared a series of V-incorporated $LiFePO_4$/C samples using a two-step solid-state reaction route. The physicochemical properties and electrochemical performances have been studied using X-ray diffraction (XRD), X-ray absorption spectroscopy (XAS), scanning electron microscopy (SEM), transmission electron microscopy (TEM), Raman spectrometry, and electrochemical measurements. The nature of vanadium incorporation in $LiFePO_4$ has been detected.

EXPERIMENTAL SECTION

Li_2CO_3, $NH_4H_2PO_4$, FeC_2O_4, and NH_4VO_3 were used as starting materials for the synthesis of nominal $LiFe_{1-x}V_xPO_4$/C. The molar ratio of Li/Fe/V/P was $1.02:(1-x):x:1.00$ ($x = 0, 0.03, 0.05, 0.07, 0.10, 0.20, 0.50, 1.00$). The materials were mixed and ground for 6 h by wet ball-milling in ethanol to ensure homogeneous mixing. The mixture was dried at 50 °C for 12 h in air, followed by calcination at 350 °C for 6 h in a nitrogen atmosphere, and then cooled down to room temperature. Glucose (5 wt %), which serves as both the reductive agent and the carbon source, was added to the resulting precursor and mixed by planetary ball-milling for 3 h in ethanol. Subsequently, the mixture was heated to 700 °C with a heating rate of 3 °C min^{-1} and was sintered for 10 h in N_2.

X-ray diffraction patterns were measured with an X'Pert Pro diffractometer (X'Pert Pro, PANalytical B.V.) using Cu Kα radiation (λ = 1.5406 Å). The morphology was observed with the scanning electron microscope (Sirion 200, Holland) and transmission electron microscope (JEM-2100, JEOL). Tap density was measured by the tap density measurement instrument (JZ-1, China).

The valences of Fe and V were investigated by X-ray absorption spectroscopy (XAS). The Fe K-edge and V K-edge XAS measurements were performed in fluorescence mode at beamline X-19A of the National Synchrotron Light Source (NSLS) at Brookhaven National Laboratory. A standard (FeO for Fe K-edge and V foil for V K-edge) was run in transmission mode simultaneously with all measurements for energy calibration. The energy resolution ($\Delta E/E$) of the X-19A beamline was 2×10^{-4}, corresponding to about 1.4 and 1.1 eV at the Fe K-edge and V K-edge, respectively. All of the XAS spectra presented in this paper were background-subtracted and normalized to unity in the continuum region about 100 eV above the edge.

Carbon coating on pristine and V-doped $LiFePO_4$/C powders was characterized by Raman spectrometry (VERTEX 70, Bruker). Carbon content was determined by dissolving samples in hydrochloric acid and keeping them boiling for 30 min, then weighing the remainder. Both pristine and V-doped $LiFePO_4$/C powders were pressed into disk-shaped pellets, and the electronic conductivity was measured by the four-point dc method.

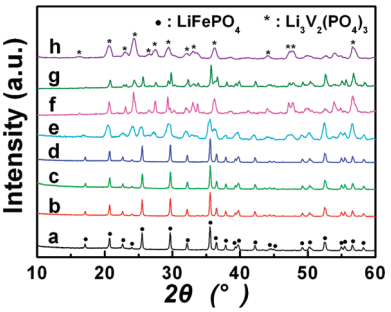

Figure 1. XRD patterns of the prepared samples with different vanadium contents: (a) 0, (b) 3, (c) 5, (d) 7, (e)10, (f) 20, (g) 50, and (h) 100 at. % vanadium.

The working electrodes were prepared by mixing active material with PVDF and acetylene black in a weight ratio of 75:15:10 in *N*-methyl pyrrolidinone solvent. The slurry of the mixture was coated on an aluminum foil (20 μm in thickness) using an automatic film-coating equipment. The resulting film was dried under an infrared light to remove volatile solvent, punched into discs (φ, 14 mm) and then pressed under a pressure of 6 MPa. After drying at 120 °C for 12 h in vacuum, the disk was transferred into an argon-filled glovebox (Super 1220/750, Mikrouna) and assembled as the working electrode in a 2025 coin cell using Celgard 2400 as the separator and lithium foil as counter and reference electrodes. A solution of 1 mol L^{-1} $LiPF_6$ in EC/DMC (LB-301, China) was employed as the electrolyte. The cells were cycled at different C rates between 2.5 and 4.2 V on a cell testing system (LAND CT2001A, China). Cyclic voltammetry (CV) measurements were performed on an electrochemical working station (PARSTAT 2273, Princeton Applied Research, America) at a slow scanning rate of 0.05 mV s^{-1} within a voltage range of 3.0−4.2 V.

RESULTS AND DISCUSSION

Figure 1 shows the XRD patterns of the as-prepared samples with different vanadium contents. All diffraction peaks of pristine $LiFePO_4$/C powders (Figure 1, pattern a) can be indexed with an ordered orthorhombic $LiFePO_4$ phase (JCPDS, No. 40-1499). For the sample with 100 at. % vanadium (Figure 1, pattern h), the diffraction peaks for monoclinic $Li_3V_2(PO_4)_3$ can be observed, though some impurities were detected, which resulted from the nonstoicheometric synthesis process of $Li_3V_2(PO_4)_3$. It was also found that there was no visible difference between the XRD patterns of pristine $LiFePO_4$ and low V-doped $LiFePO_4$/C (3−7 at. % V) (Figure 1, patterns b−d), indicating that V had been doped into the host lattice or the amount of the composites formed from vanadium had been too low. In contrast, for those high-level V-doped $LiFePO_4$/C samples (10−50 at. % V) (Figure 1, patterns e−g), the peaks of $Li_3V_2(PO_4)_3$ impurities could be also distinctly detected. A full Rietveld refinement was carried out on $LiFePO_4$/C, $LiFe_{0.97}V_{0.03}PO_4$/C, and $LiFe_{0.95}V_{0.05}PO_4$/C samples, and the results are listed in Table 1. The best refinement model was chosen from a *Pnma* space group. Satisfactory and acceptable reliability factors ($R_{wp} < 12$, $S < 2$) are only obtained for $LiFePO_4$/C and $LiFe_{0.97}V_{0.03}PO_4$/C. However, for $LiFe_{0.95}V_{0.05}PO_4$/C, the reliability factor, R_{wp}, is greater than 12, indicating

Table 1. Lattice Parameters of $LiFePO_4$, $LiFe_{0.97}V_{0.03}PO_4$, and $LiFe_{0.95}V_{0.05}PO_4$

sample		$LiFePO_4$	$LiFe_{0.97}V_{0.03}PO_4$	$LiFe_{0.95}V_{0.05}PO_4$
lattice constant (Å)	a	10.3334(10)	10.3330(10)	10.3286(10)
	b	6.0102(6)	6.0100(6)	6.0073(6)
	c	4.6962(5)	4.6975(5)	4.6962(5)
lattice volume (Å^3)		291.66(5)	291.72(5)	291.38(5)
interatomic distance (Å)	Li−O_1	2.0933	2.0935	2.0929
	Li−O_2	2.1623	2.1625	2.1618
	Li−O_3	2.1928	2.1930	2.1923
	Li−O_{mean}	2.1495	2.1497	2.1490
reliability factors (%)	R_{wp}	11.87	10.64	12.35
	R_p	8.92	8.36	9.38
	S	1.23	1.35	1.20

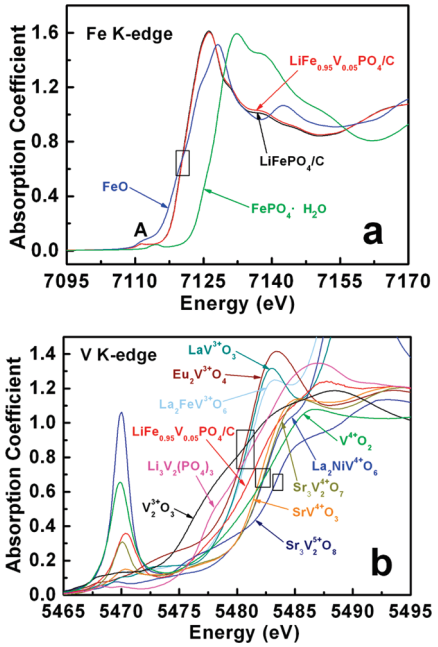

Figure 2. XAS spectra of pristine and 5 at. % V-doped $LiFePO_4$/C powders.

that it is not appropriate to use only the *Pnma* space group for refinement. A second phase could also exist, and a new refinement model should be created in the meantime. Because of the complexity of refinement on multiphases, the refinement was not carried out on other V-doped $LiFePO_4$/C samples. When comparing $LiFe_{0.97}V_{0.03}PO_4$ with $LiFePO_4$, the c axis elongates, but a and b axes shrink, resulting in an enlarged lattice volume for $LiFe_{0.97}V_{0.03}PO_4$. In addition, the incorporation of vanadium results in the Li−O bond lengthening, indicating that the Li ions would intercalate or deintercalate more easily. The changes in lattice parameters prove that V was doped into the host lattice. It is worth noting that no diffraction peaks from carbon were detected, which indicates that the residual carbon is amorphous or the carbon layer on LFP particles is too thin.

In Figure 2a, the Fe K-edge spectra for the pristine $LiFePO_4$/C and the $LiFe_{0.95}V_{0.05}PO_4$/C samples are shown along with the spectra of reference compounds $Fe^{2+}O$ and $Fe^{3+}PO_4 \cdot H_2O$ for comparison. The spectra for the pristine and V-doped samples are almost identical, indicating that the valence value for Fe is the same for both of them. The primary indicator of valence variation is the chemical shift in the main portion of the edge to higher energy with increasing valence. Figure 2a clearly shows that the values of the edge energies (defined as the energy at absorption coefficient $\mu \sim 0.5$) are almost the same (~7119 eV) for $LiFePO_4$/C, $LiFe_{0.95}V_{0.05}PO_4$/C, and $Fe^{2+}O$ but are shifted about 6 eV below the edge for the Fe^{3+} compound, that is, $Fe^{3+}PO_4 \cdot H_2O$. This leads to the assignment of a Fe^{2+} for $LiFePO_4$/C and $LiFe_{0.95}V_{0.05}PO_4$/C. The pre-edge feature (labeled by letter A) located at about 7112 eV involves 1s → 3d quadrupole transitions and 1s → p/3d hybridized states via dipole transitions. The weakness of the pre-edge feature is consistent with the centrosymmetric octahedral sites. The low onset energy of the A feature[39−41] also supports the Fe^{2+} valence[41] in the $LiFePO_4$-based materials. (The A feature of the $Fe^{3+}PO_4 \cdot H_2O$ is shifted up in energy.) Thus, both the main- and pre-edge portions of the Fe K-edge XAS spectra clearly confirm that the valence state of Fe in the pristine and V-doped $LiFePO_4$ samples is Fe^{2+}. Therefore, V incorporation in $LiFePO_4$/C does not change the valence state of Fe ions.

Figure 2b shows the V K-edge XAS spectra for $LiFe_{0.95}V_{0.05}PO_4$/C and related reference compounds. The formal valence values for V are +3 for standards V_2O_3, La_2FeVO_6, Eu_2VO_4, $Li_3V_2(PO_4)_3$, and $LaVO_3$; +4 for VO_2, $SrVO_3$, $Sr_3V_2O_7$, and La_2NiVO_6; and +5 for $Sr_3V_2O_8$. It can be seen that the edge energy increases with the increase of valence from +3 to +5. The edge energy for $LiFe_{0.95}V_{0.05}PO_4$/C is between those of trivalent and tetravalent V compounds, revealing that the valence of V in this $LiFe_{0.95}V_{0.05}PO_4$/C specimen should be between +3 and +4. The pre-edge features of V compounds are too complicated to interpret due to the stronger d/p hybridization that accompanies the larger spatial extent of the V 3d states.

SEM images of pristine and corresponding typical V-doped $LiFePO_4$/C powders under study are shown in Figure 3. V doping slightly changes the particle size and morphology. For example, the particle size of pristine and V-doped $LiFePO_4$/C powders is between ~50 and 500 nm (Figure 3a−d), whereas the sample with 100 at. % vanadium presents irregular blocks with a wide size distribution ranging from ~20 nm to 1.0 μm (Figure 3e).

TEM images of pristine and 5 at. % V-doped $LiFePO_4$/C powders are shown in Figure 4. Both pristine and 5 at. % V-doped $LiFePO_4$/C samples present a typical core−shell structure with an amorphous carbon wrapping or connecting of the $LiFePO_4$ particles. The thickness of the carbon layer is about 2−4 nm, which is favorable to enhance the conductivity but does not affect intercalation/deintercalation of Li^+ because the Li^+ ions can readily penetrate through the thin carbon layer.

Tap density is an important parameter for the cathode materials. The theoretical density of $LiFePO_4$ is higher than that of $Li_3V_2(PO_4)_3$. In our case, the tap density of $Li_3V_2(PO_4)_3$/C (1.13 g cm^{-3}) is lower than that of $LiFePO_4$/C (1.27 g cm^{-3}), but 5% V-doped $LiFePO_4$/C shows a higher tap density (1.37 g cm^{-3}). With further increasing the V content, the tap density becomes lower (for example, 1.19 g cm^{-3} for 10% V-doped $LiFePO_4$/C and 1.17 g cm^{-3} for 20% V-doped $LiFePO_4$/C). It can be concluded that a small amount of V incorporation can enhance the tap density because a limited V can enter into the lattice of $LiFePO_4$. Excessive V incorporation may decrease the tap density due to the formation of more $Li_3V_2(PO_4)_3$ phase in $LiFePO_4$.

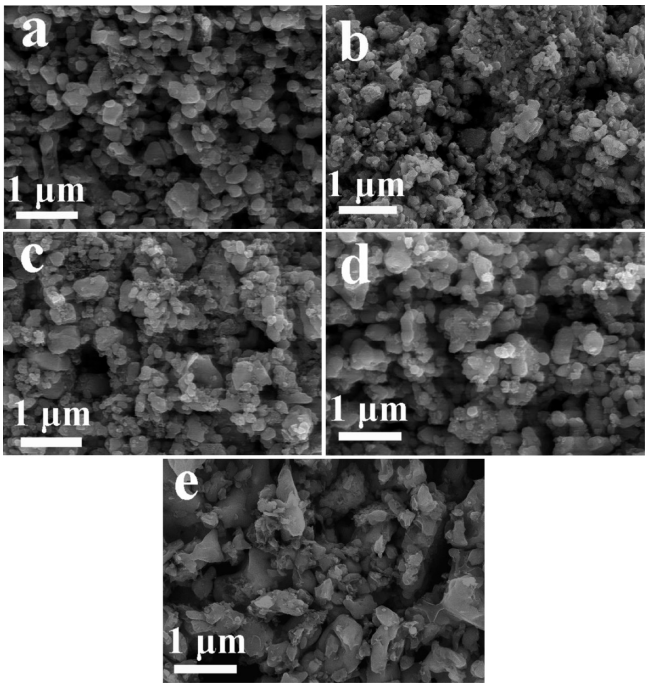

Figure 3. SEM images of pristine and several typical V-doped $LiFePO_4$/C: (a) 0, (b) 3, (c) 5, (d) 20, and (e) 100 at. % vanadium.

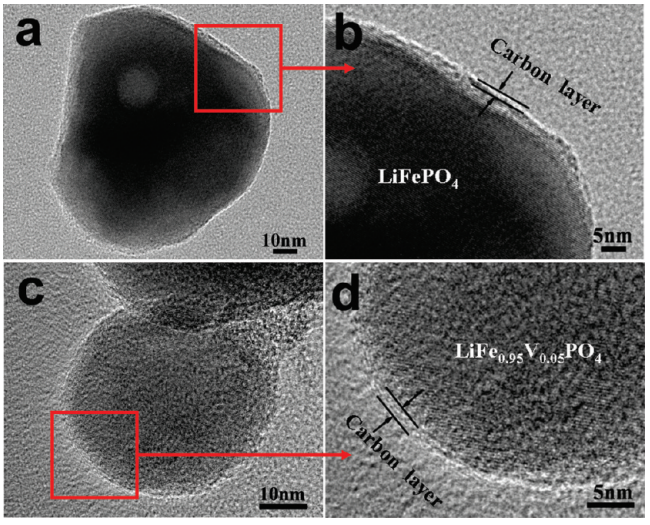

Figure 4. TEM images of samples: (a, b) pristine and (c, d) 5 at. % V-doped $LiFePO_4$/C particles.

CV profiles reflect the electrochemical properties of not only the active material but also the entire electrode. Considering the effect of electrode loading (thickness) on CV behaviors, the electrodes with the same thickness (20 μm) were used for CV tests, and a slow scanning rate of 0.05 mV s^{-1} was employed. The CV profiles of all samples are shown in Figure 5. Only one anodic peak and one cathodic peak at ~3.35 and ~3.52 V, corresponding to the phase-transition process between $LiFePO_4$ and $FePO_4$, are observed in the CV profiles of both pristine $LiFePO_4$ and the 3 at. % V-doped $LiFePO_4$ samples, which again indicates that V is doped into the host lattice when its content is low. For the sample with 100 at. % vanadium, three redox potential pairs around 3.60/3.57, 3.70/3.65, and 4.10/4.02 V are observed. This is consistent with the results previously reported for $Li_3V_2(PO_4)_3$.[25,28] In the range of 3.0−4.2 V, $Li_3V_2(PO_4)_3$ can intercalate/deintercalate two Li^+ ions reversibly based on the V^{3+}/V^{4+} redox couple.[25−27] The two anodic peaks observed at 3.60 and 3.70 V correspond to the deintercalation of the first Li^+ with two steps while the second Li^+ is removed via a single step corresponding to the last anodic peak observed at 4.10 V.[25] In contrast, for V-incorporated samples (x = 0.05, 0.07, 0.10, 0.20, 0.50), not only the redox potential peak of $LiFePO_4$ but also the three redox potentials of $Li_3V_2(PO_4)_3$ are observed, which matches well with those of $Li_3V_2(PO_4)_3$/$LiFePO_4$ composites.[28,29] To our knowledge, the three visible redox potential peaks simultaneously appear only if vanadium exists in the form of $Li_3V_2(PO_4)_3$. Nevertheless, combined with the valence between +3 and +4 of V in the $LiFe_{0.95}V_{0.05}PO_4$ specimen from XAS analysis, it is reasonable to speculate that, when the vanadium content reaches its limit in the host lattice, the excessive vanadium has to form $Li_3V_2(PO_4)_3$ and $LiVOPO_4$, whose valences are +3 and +4, respectively. The redox potential waves around 4.0 V are supposed to be the overlapping peaks of $LiVOPO_4$ and $Li_3V_2(PO_4)_3$. Conclusively, the CV profiles of the V-doped samples (x = 0.05, 0.07, 0.10, 0.20, 0.50) observed here are simply superimposed profiles of $LiFePO_4$, $Li_3V_2(PO_4)_3$, and $LiVOPO_4$. It is reasonable to assume that V-doped $LiFePO_4$, $Li_3V_2(PO_4)_3$, and $LiVOPO_4$ coexist in the samples with high V-doping contents (x = 0.05, 0.07, 0.10, 0.20, 0.50). Compared with other samples, especially pristine $LiFePO_4$/C, the 5 at. % V-doped sample shows not only well-defined and finely symmetric peaks but also a smaller difference between reduction and oxidation potentials (0.17 V). This indicates that the electrode reaction has a higher speed constant and a better reversibility of the Li^+ extraction/insertion reactions. Furthermore, according to the Randles Sevcik equation[42]

$$I_p = 2.69 \times 10^5 n^{3/2} A D^{1/2} v^{1/2} C$$

where I_p is the CV peak current (A), n is the number of electrons involved in the redox process, A is the electrode area (cm^2), D is the Li^+ diffusion coefficient (cm^2 s^{-1}), v is the potential scan rate (V s^{-1}), and C is the shuttle concentration (mol cm^{-3}). The stronger the CV currents are, the larger the Li^+ diffusion coefficients are. For the 5 at. % V-doped sample, the CV profile exhibits the highest peak current, which facilitates the kinetic process of the electrochemical reactions, indicative of a better electrochemical performance.

The specific capacities of samples were measured by a constant current charge/discharge test between 2.5 and 4.2 V (vs Li^+/Li). The discharge characteristics of the first cycle at 0.1 C and the cyclic performances at different C rates are shown in Figures 6 and 7, respectively. As seen in the profiles of V-doped samples (x = 0.05, 0.07, 0.10, 0.20, 0.50) (Figure 6), not only a couple of charge/discharge plateaus at ~3.52/3.35 V for intercalation/deintercalation of Li^+ into/from $LiFePO_4$ but also three typical charge/discharge plateaus around 3.60/3.57, 3.70/3.65, and 4.10/4.02 V for intercalation/deintercalation of two Li^+ reversibly into/from $Li_3V_2(PO_4)_3$ based on the V^{3+}/V^{4+} redox couple are distinctly observed, which matches well with the charge/discharge profiles of $Li_3V_2(PO_4)_3$/$LiFePO_4$ composites[28,29,38] and agrees well with the CV profiles shown in Figure 5. The charge/discharge plateau of $LiVOPO_4$ is regarded to be overlapped with that of $Li_3V_2(PO_4)_3$ around 4.0 V. Furthermore, the vanadium content is found to have a dramatic effect on the

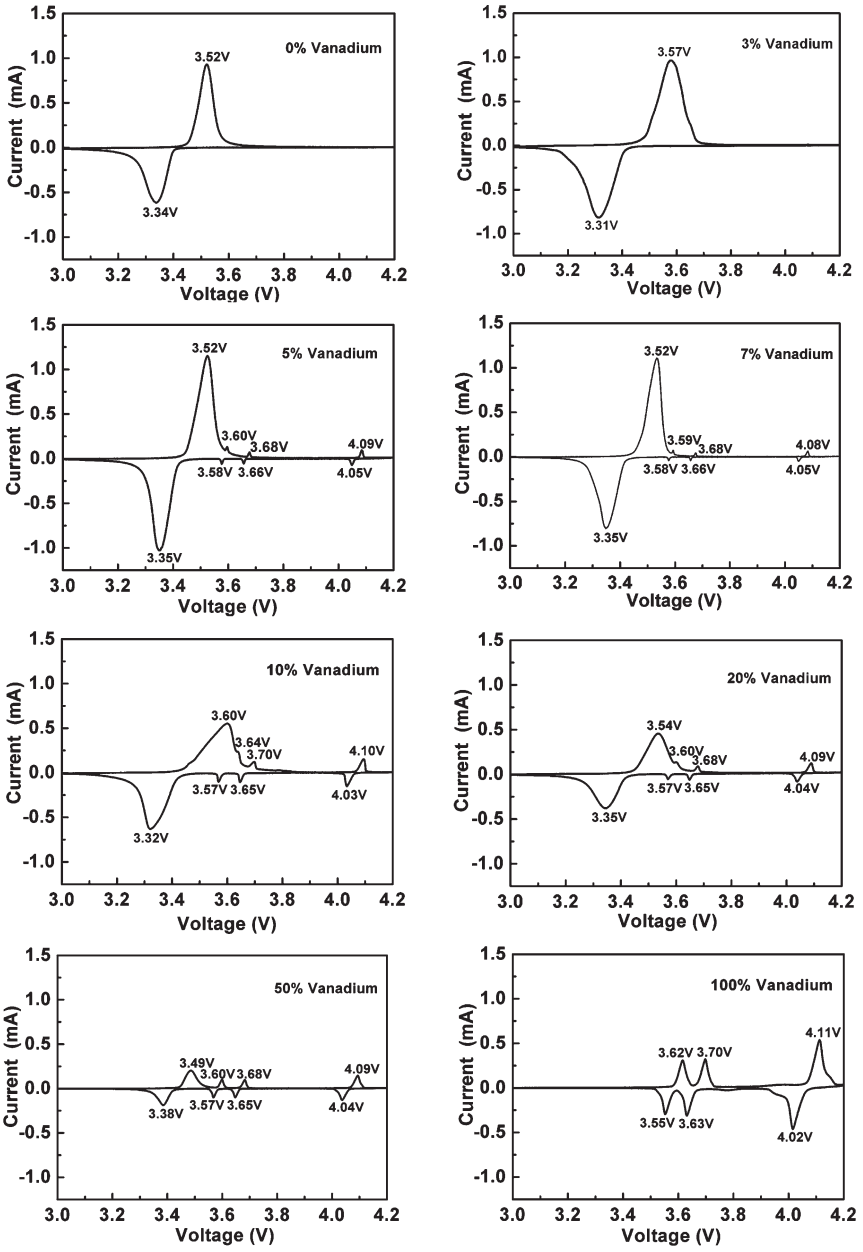

Figure 5. CV profiles of the samples at the scanning rate of 0.05 mV s^{-1} and in a potential window of 3.0−4.2 V (vs Li^+/Li).

electrochemical performances of the compound under study. The capacities of the V-doped samples increase gradually at all rates with the increase of vanadium content until the amount of vanadium was more than 5 at. %, because not only the $Li_3V_2(PO_4)_3$ with a higher theoretic capacity could enhance the electronic conductivity of the $LiFePO_4$[32,38] but also the open three-dimensional (3D) framework of $Li_3V_2(PO_4)_3$ results in faster Li^+ migration than that of $LiFePO_4$.[25,26] The 5 at. % V-doped sample shows the best electrochemical performance, approaching 159 and 125 mAh g^{-1} at 0.1 and 5.0 C for the first cycle with a capacity retention ratio (Table 2) of more than 97.5% at all rates. From Table 2, we can also observe that the rate capability is significantly enhanced with V incorporation, and the 5 at. % V-doped sample exhibits the highest capacity at high rates (e.g., the specific discharge capacity at the 50th cycle is 129 mAh g^{-1} at 5.0 C). Moreover, as shown in Figure 6, the 5 at. % V-doped sample exhibits a stable and broad charge/discharge plateau. Its charge plateau shifts to the negative direction and the discharge plateau to the positive, indicating that the sample has a relatively less voltage hysteresis than others. Obviously, the electrochemical performance of $LiFePO_4$ can be remarkably enhanced by incorporation of a low amount of $Li_3V_2(PO_4)_3$, which further corroborates the conclusions in the literature.[28,29,38] The capacities of other samples with higher vanadium contents (7−100 at. %) decreased gradually, and the sample with 100 at. % vanadium showed a notably poor electrochemical performance compared with $Li_3V_2(PO_4)_3$,[25,26,29] resulting from the nonstoicheometric synthesis process of $Li_3V_2(PO_4)_3$.

Table 3 shows the carbon content and electronic conductivity of the as-prepared $LiFe_{1-x}V_xPO_4/C$ ($x = 0, 0.03, 0.05, 0.07, 0.10, 0.20, 0.50, 1.00$). It is found that the carbon content decreases with the increase of the vanadium content, because the pyrolytic

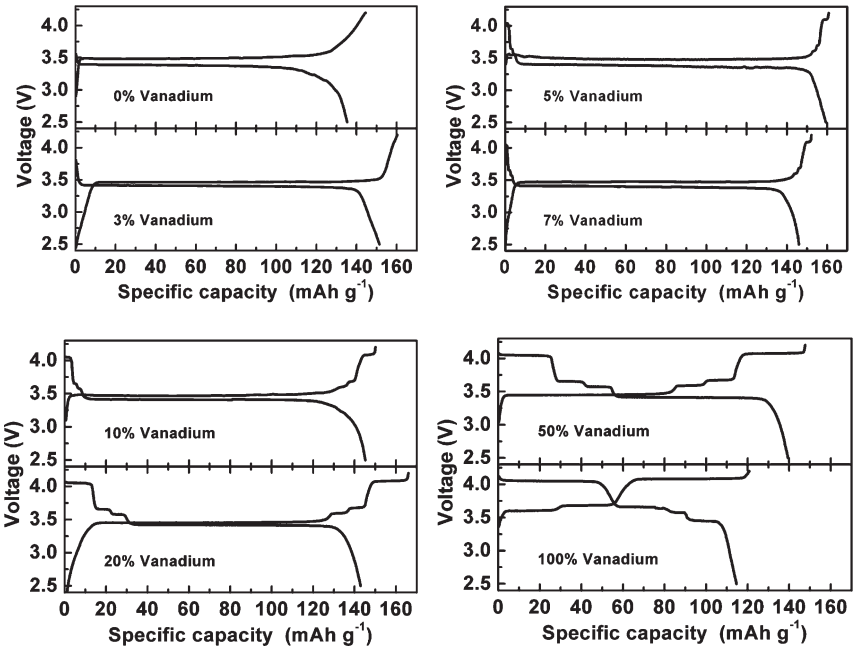

Figure 6. Charge/discharge profiles of samples at 0.1 C.

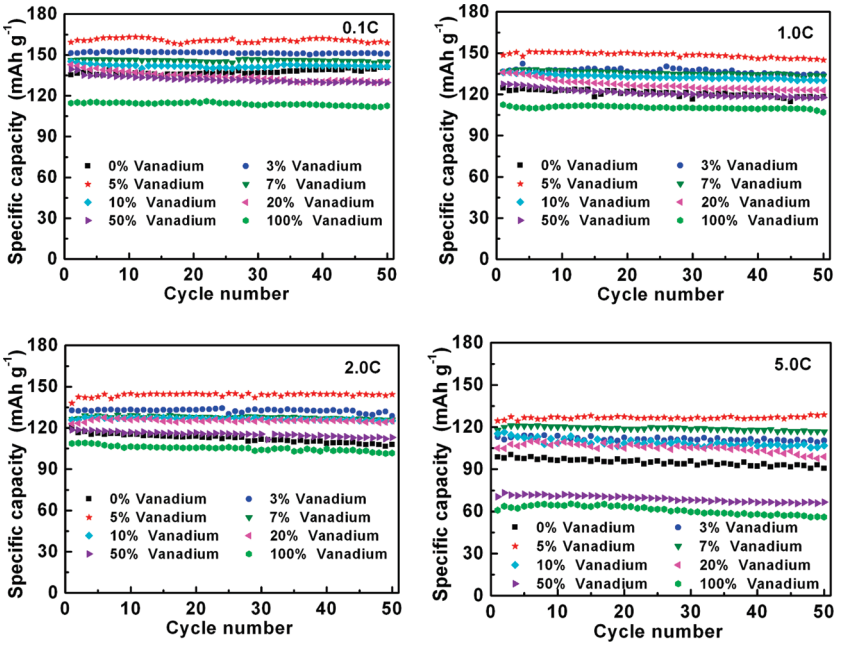

Figure 7. Cyclic performances of samples at different C rates (0.1, 1.0, 2.0, 5.0 C).

carbon was increasingly consumed for the reduction of V^{5+} to V^{3+} during the synthesis process. However, the electronic conductivity of the V-doped samples is higher than that of $LiFePO_4$ when the vanadium content is less than 7 at. % because $Li_3V_2(PO_4)_3$ impurities could enhance the electronic conductivity of $LiFePO_4$,[28,38] but the electronic conductivity of the V-doped samples gradually decreases. This is because the electronic conductivity of the samples depends mainly on the residual carbon content rather than the vanadium content. It is well known that the higher electronic conductivity is , the better the electrochemical performance is. However, in our measurement, it is found that the sample with the best electrochemical performance is not the 3 at. % V-doped sample that has the highest electronic conductivity (7.48×10^{-3} S cm^{-1}), but the 5 at. % V-doped sample that has a relatively lower electronic conductivity (6.72×10^{-4} S cm^{-1}). This is caused by the excessive carbon and the low doping level of vanadium. The excessive carbon would be a barrier for the diffusion of Li^+ ions during the charge/discharge process, and the inactive carbon would reduce the ratio of the active material, leading to a decrease in capacity. On the other hand, when the amount of vanadium is too low, it is not easy to form $Li_3V_2(PO_4)_3$ with higher electronic conductivity and higher

dx.doi.org/10.1021/jp2034906 |J. Phys. Chem. C 2011, 115, 13520–13527

Table 2. Discharge Capacities of the 1st and the 50th Cycles at Different C Rates of the Samples

	0.1 C (mAh g^{-1})			1.0 C (mAh g^{-1})			2.0 C (mAh g^{-1})			5.0 C (mAh g^{-1})		
	1st	50th	R (%)[a]	1st	50th	R (%)[a]	1st	50th	R (%)[a]	1st	50th	R (%)[a]
0% V	135.3	140.9	104.1	124.7	118.3	94.9	120.2	107.9	89.8	98.7	90.6	91.8
3% V	151.4	150.9	99.7	136.6	134.5	98.5	132.7	128.7	97.0	113	110.4	97.70
5% V	159.4	159.0	99.7	148.7	145.0	97.5	138	144.4	104.6	124.6	128.8	103.4
7% V	146.1	145	99.3	136.5	133.4	97.7	126.3	125.9	99.78	117.8	116.7	99.1
10% V	145.2	141.5	97.5	136	130.1	95.6	125.9	125.2	99.4	115.4	106.8	92.5
20% V	142.9	130.3	91.2	135.9	123	90.5	123.1	125.1	101.6	105	98.9	94.2
50% V	139.4	129.8	93.1	127.5	117.8	92.4	118.7	113.1	95.3	70.4	66.6	94.6
100% V	114.6	112.6	98.3	112.5	107	95.1	108.7	101.7	93.6	60.9	56	92.0

[a] Capacity retention ratios compared to the first cycle.

Table 3. Carbon Content and Electronic Conductivity of the As-Prepared Samples

sample	carbon content (wt. %)	electronic conductivity (S cm^{-1})
LFP	3.43	$<10^{-6}$
3% V	3.27	7.48×10^{-3}
5% V	3.14	6.72×10^{-4}
7% V	2.94	8.54×10^{-5}
20% V	2.88	$<10^{-6}$
50% V	2.65	$<10^{-6}$
100% V	2.62	$<10^{-6}$

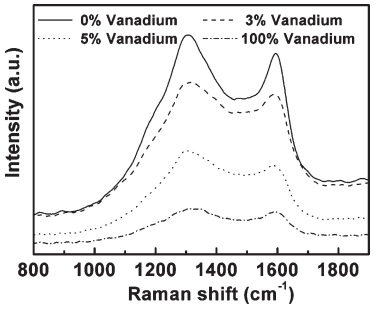

Figure 8. Raman spectra of the samples.

capacity. Thus, it can be concluded that the enhancement of the electrochemical performance should be mainly due to the existence of a small amount of $Li_3V_2(PO_4)_3$ rather than the doping of V in the host lattice.

Raman spectroscopy is useful for estimating the carbon coating on $LiFePO_4$ powders.[43−46] As shown in Figure 8, two intense broad bands (~1305 and 1590 cm^{-1}) are assigned to the disordered (D) and graphene (G) bands of the residual carbon in the samples, respectively. Because the relative width and intensity of the D and G bands are related to the growth and size of different carbon phases and the presence of functional groups and impurities, the D/G ratio is useful for comparing samples to each other but is not a quantitative measure of the graphene and the disordered carbon structure.[45] As shown in Figure 8, the positions of D and G bands shift slightly among these samples, and their intensity ratios change distinctly. The lower the intensity ratio of D and G bands is, the higher the electronic conductivity of the residual carbon is.[43−46] However, in this study, the integrated Raman intensity ratios of D and G bands of the samples decrease in the order of carbon content with the increase in vanadium content, which indicates that the degree of graphitization of the residual carbon is enhanced with the increase of vanadium content. However, the intensity ratios are not in agreement with the electronic conductivity of samples, because the electronic conductivity of the samples depends not only on the residual carbon but also on the vanadium content. Furthermore, the small intensity ratios of PO_4 (953 cm^{-1}) and carbon bands in Figure 8 indicate a more uniform carbon coating on the surface of samples, resulting in better electrochemical properties.

CONCLUSIONS

$LiFePO_4$/C samples with different vanadium contents were successfully prepared via a two-step sintering route. The effect of vanadium incorporation on the performance of $LiFePO_4$ has systematically been investigated with X-ray diffraction (XRD), Raman, charge/discharge measurements, and cyclic voltammetry (CV) tests. It shows that $Li_3V_2(PO_4)_3$ could enhance the electronic conductivity of $LiFePO_4$, due to the increasing degree of graphitization of the residual carbon with vanadium introduction. Moreover, the open three-dimensional (3D) framework of $Li_3V_2(PO_4)_3$ can result in a faster lithium-ion migration than that of $LiFePO_4$. Accordingly, the electrochemical performance of $LiFePO_4$/C is enhanced by introducing vanadium. The vanadium incorporation is found to have a dramatic effect on electrochemical performance. The $LiFePO_4$/C sample with 5 at. % vanadium doping is found to exhibit the best electrochemical performance with a specific discharge capacity of 129 mAh g^{-1} at 5.0 C after 50 cycles; the capacity retention ratio is higher than 97.5% at all C rates from 0.1 to 5.0 C. The XAS results show that the valence of V in the $LiFe_{0.95}V_{0.05}PO_4$/C specimen is between +3 and +4. Combined with XRD, charge/discharge profiles, and CV tests, it is shown that vanadium can be doped into the host lattice when the doping level of vanadium is low ($x \leq 0.03$), whereas excessive vanadium can form $Li_3V_2(PO_4)_3$ and $LiVOPO_4$ impurities at higher doping levels ($0.05 \leq x < 1.00$). Our results clarified the nature of V doping into $LiFePO_4$ and are helpful for understanding the enhancement mechanism of the electrochemical performance of $LiFePO_4$.

AUTHOR INFORMATION

Corresponding Author

*Tel: +86-27-87558241. Fax: +86-27-87558241. E-mail: huangyh@mail.hust.edu.cn.

■ ACKNOWLEDGMENT

This work was financially supported by the National Excellent Young Scientists Fund of China (No. 50825203), 863-National High Technology Research and Development Program of China (Nos. 2009AA03Z225 and 2011AA11290), National Science Foundation under Grants (No. CHE-0718482), an award from the Research Corporation for Science Advancement, and an ERG grant from Sam Houston State University. In addition, the authors thank the Analytical and Testing Center of Huazhong University of Science and Technology for providing XRD, SEM, Raman spectra measurements.

■ REFERENCES

(1) Padhi, A. K.; Nanjundaswamy, K. S.; Goodenough, J. B. *J. Electrochem. Soc.* **1997**, *144*, 1188–1194.
(2) Yuan, L. X.; Wang, Z. H.; Zhang, W. X; Hu, X. L.; Chen, J. T.; Huang, Y. H.; Goodenough, J. B. *Energy Environ. Sci.* **2011**, *4*, 269–284.
(3) Huang, Y. H.; Goodenough, J. B. *Chem. Mater.* **2008**, *20*, 7237–7241.
(4) Wang, G.; Liu, H.; Liu, J.; Qiao, S.; Lu, G. M.; Munro, P.; Ahn, H. *Adv. Mater.* **2010**, *42*, 4944–4948.
(5) Ravet, N.; Chouinard, Y.; Magnan, J. F.; Besner, S.; Gauthier, M.; Armand, M *J. Power Sources* **2001**, *97*−*98*, 503–507.
(6) Prosini, P. P.; Zane, D.; Pasquali, M. *Electrochim. Acta* **2001**, *46*, 3517–3523.
(7) Chung, S.-Y.; Bloking, J. T.; Chiang, Y.-M. *Nat. Mater.* **2002**, *1*, 123–128.
(8) Park, K. S.; Son, J. T.; Chung, H. T.; Kim, S. J.; Lee, C. H.; Kang, K. T.; Kim, H. G. *Solid State Commun.* **2004**, *129*, 311–314.
(9) Oh, S. W.; Myung, S.-T.; Oh, S.-M.; Oh, K. H.; Amine, K.; Scrosati, B.; Sun, Y.-K. *Adv. Mater.* **2010**, *22*, 4842–4845.
(10) Zhao, J.; He, J.; Zhou, J.; Guo, Y.; Wang, T.; Wu, S.; Ding, X.; Huang, R.; Xue, H. *J. Phys. Chem. C* **2011**, *115*, 2888–2894.
(11) Gaberscek, M.; Dominko, R.; Jamnik, J. *Electrochem. Commun.* **2007**, *9*, 2778–2783.
(12) Delmas, C.; Maccario, M.; Croguennec, L.; Le Cras, F.; Weill, F. *Nat. Mater.* **2008**, *7*, 665–671.
(13) Mestre-Aizpurua, F.; Hamelet, S.; Masquelier, C.; Palacin, M. R. *J. Power Sources* **2010**, *195*, 6897–6901.
(14) Wang, D.; Li, H.; Shi, S.; Huang, X.; Chen, L. *Electrochim. Acta* **2005**, *50*, 2955–2958.
(15) Herle, P. S.; Ellis, B.; Coombs, N.; Nazar, L. F. *Nat. Mater.* **2004**, *3*, 147–152.
(16) Hong, J.; Wang, C. S.; Chen, X.; Upreti, S.; Whittingham, M. S. *Electrochem. Solid-State Lett.* **2009**, *12*, A33–A38.
(17) Lee, K. T.; Lee, K. S. *J. Power Sources* **2009**, *189*, 435–439.
(18) Ouyang, C. Y.; Shi, S. Q.; Wang, Z. X.; Li, H.; Huang, X. J.; Chen, L. Q. *J. Phys.: Condens. Matter* **2004**, *16*, 2265–2272.
(19) Sakamoto, J. S.; Dunn, B. *J. Mater. Chem.* **2002**, *12*, 2859–2861.
(20) Le Meins, J.-M.; Crosnier-Lopez, M.-P.; Hemon-Ribaud, A.; Courbion, G. *J. Solid State Chem.* **1999**, *148*, 260–277.
(21) Gover, R. K. B.; Bryan, A.; Burns, P.; Barker, J. *Solid State Ionics* **2006**, *177*, 1495–1500.
(22) Song, Y.; Zavalij, P. Y.; Whittingham, M. S. *J. Electrochem. Soc.* **2005**, *152*, A721–728.
(23) Barker, J.; Saïdi, M. Y.; Swoyer, J. L. *J. Electrochem. Soc.* **2003**, *150*, A1394–A1398.
(24) Gaubicher, J.; Le Mercier, T.; Chabre, Y.; Angenault, J.; Quarton, M. *J. Electrochem. Soc.* **1999**, *146*, 4375–4379.
(25) Saïdi, M. Y.; Barker, J.; Huang, H.; Swoyer, J. L.; Adamson, G. *Electrochem. Solid-State Lett.* **2002**, *5*, A149–A151.
(26) Saïdi, M. Y.; Barker, J.; Huang, H.; Swoyer, J. L.; Adamson, G. *J. Power Sources* **2003**, *119*−*121*, 266–272.
(27) Yin, S. C.; Grondey, H.; Strobel, P.; Hunag, H.; Nazar, L. F. *J. Am. Chem. Soc.* **2003**, *125*, 326–327.
(28) Yang, M. R.; Ke, W. H.; Wu., S. H. *J. Power Sources* **2007**, *165*, 646–650.
(29) Zheng, J. C.; Li, X. H.; Wang, Z. X.; Li, J. H.; Li, L. J.; Wu, L.; Guo, H. J. *Ionics* **2009**, *15*, 753–759.
(30) Wen, Y. X.; Zeng, L. M.; Tong, Z. F.; Nong, L. Q.; Wei, W. X. *J. Alloys Compd.* **2006**, *416*, 206–208.
(31) Liu, H.; Li, C.; Cao, Q.; Wu, Y. P.; Holze, R. *J. Solid State Electrochem.* **2008**, *12*, 1017–1020.
(32) Yang, M. R.; Ke, W. H. *J. Electrochem. Soc.* **2008**, *155*, A729–A732.
(33) Sun, C. S.; Zhou, Z.; Xu, Z. G.; Wang, D. G.; Wei, J. P.; Bian, X. K.; Yan, J. *J. Power Sources* **2009**, *193*, 841–845.
(34) Hong, J.; Wang, C. S.; Chen, X.; Upreti, S.; Whittingham, M. S. *Electrochem. Solid-State Lett.* **2009**, *12*, A33–A38.
(35) Wu, Z. J.; Yue, H. F.; Li, L. S.; Jiang, B. F.; Wu, X. R.; Wang, P. *J. Power Sources* **2010**, *195*, 2888–2893.
(36) Jin, Y.; Yang, C. P.; Rui, X. H.; Cheng, T.; Chen, C. H. *J. Power Sources* **2011**, *196*, 5623−5630.
(37) Ma, J.; Li, B.; Du, H.; Xu, C.; Kang, F. *J. Electrochem. Soc.* **2011**, *158*, A26–A32.
(38) Wang, L. N.; Li, Z. C.; Xu, H. J.; Zhang, K. L. *J. Phys. Chem. C* **2008**, *112*, 308–312.
(39) Liang, G.; Park, K.; Li, J.; Benson, R.; Vaknin, D.; Markert, J. T.; Croft, M. *Phys. Rev. B* **2008**, *77*, 064414.
(40) Haas, O.; Deb, A.; Cairns, E. J.; Workaun, A. *J. Electrochem. Soc.* **2005**, *152*, A191–A196.
(41) Westre, T. E.; Kennepohl, P.; DeWitt, J. G.; Hedman, B.; Hodgson, K. O.; Solomon, E. I. *J. Am. Chem. Soc.* **1997**, *119*, 6297–6314.
(42) Dahn, J. R.; Jiang, J. W.; Moshurchak, L. M. *J. Electrochem. Soc.* **2005**, *152*, A1283–1289.
(43) Doeff, M. M.; Hu, Y. Q.; McLarnon, F.; Kostecki, R. *Electrochem. Solid-State Lett.* **2003**, *6*, A207–A209.
(44) Nakamura, T.; Miwa, Y.; Tabuchi, M.; Yamada, Y. *J. Electrochem. Soc.* **2006**, *153*, A1108–A1114.
(45) Wilcox, J. D.; Doeff, M. M.; Marcinek, M.; Kostecki, R. *J. Electrochem. Soc.* **2007**, *154*, A389–A395.
(46) Baddour-Hadjean, R.; Pereira-Ramos, J.-P. *Chem. Rev.* **2010**, *110*, 1278–1319.